coatings

MDPI

Article

Effect of Sensitization on the Electrochemical Properties of Nanostructured NiO

Matteo Bonomo [1,*], Daniele Gatti [1], Claudia Barolo [2,3] and Danilo Dini [1,*]

1 Department of Chemistry, University of Rome "La Sapienza", p.le A. Moro 5, 00185 Rome, Italy; daniele.gatti127@gmail.com
2 Department of Chemistry, NIS Interdepartmental Centre and INSTM Reference Centre, University of Turin, via Pietro Giuria 7, 10125 Torino, Italy; claudia.barolo@unito.it
3 ICxT Interdepartmental Centre, Lungo Dora Siena 100, 10153 Torino, Italy
* Correspondence: matteo.bonomo@uniroma1.it (M.B.); danilo.dini@uniroma1.it (D.D.); Tel.: +39-06-4991-3335 (D.D.)

Received: 7 February 2018; Accepted: 25 June 2018; Published: 29 June 2018

Abstract: Screen-printed NiO electrodes were sensitized with 11 different dyes and the respective electrochemical properties were analyzed in a three-electrode cell with the techniques of cyclic voltammetry and electrochemical impedance spectroscopy. The dye sensitizers of NiO were organic molecules of different types (e.g., squaraines, coumarins, and derivatives of triphenyl-amines and erythrosine B), which were previously employed as sensitizers of the same oxide in dye-sensitized solar cells of *p*-type (*p*-DSCs). Depending on the nature of the sensitizer, diverse types of interactions occurred between the immobilized sensitizer and the screen-printed NiO electrode at rest and under polarization. The impedance data recorded at open circuit potential were interpreted in terms of two different equivalent circuits, depending on the eventual presence of the dye sensitizer on the mesoporous electrode. The fitting parameter of the charge transfer resistance through the electrode/electrolyte interface varied in accordance to the differences of the passivation action exerted by the various dyes against the electrochemical oxidation of NiO. Moreover, it has been observed that the resistive term R_{CT} associated with the process of dark electron transfer between the dye and NiO substrate is strictly correlated to the overall efficiency of the photoconversion (η) of the corresponding *p*-DSC, which employs the same dye-sensitized electrode as photocathode.

Keywords: nickel oxide; organic sensitizers; dye-sensitized solar cells

1. Introduction

p-type nickel oxide (NiO) [1,2]; is widely employed as electrodic material in photoelectrochemical cells [3–9], electrochromic windows [10–14], and charge storage systems [15–17], among others [18–20]. The wide range of NiO applicability derives from the fact that NiO can constitute a functional material in both bulk [21] and nanostructured [22,23] versions. When nanostructured NiO is employed in the configuration of thin film (thickness, l < 10 μm) it displays photoelectrochemical activity in the presence of opportune redox mediators (e.g., the redox couple I^-/I_3^-) [24]. Moreover, nanostructured films of NiO present solid-state electroactivity [25–27] due to the verification of a series of reversible electrochemical processes that switch the properties of electrical transport [28] and optical absorption [29] of the oxide itself. The optical [10–14,30,31], magnetic [32,33], electrochemical [34], and photoelectrochemical [35,36] properties of NiO (either in the bulk state or in the nanostructured version) are considerably altered when the surface of the oxide is dye-sensitized [37]. Such a type of electrode modification consists mainly in the impartation of additional optical absorption [38–49] and photoelectroactivity to NiO in the NIR-Vis range, i.e., in a spectral range of lower energies with

respect to the intrinsic optical absorption of pristine NiO (typically in the near ultraviolet (UV)) [50]. Dye sensitization of nanostructured *p*-type NiO is finalized principally to the realization of devices, such as dye-sensitized solar cells of *p*-type (*p*-DSCs) [51–59], light-fueled electrolyzers for hydrogen generation [5,60–65], and photoelectrochemical reactors for carbon dioxide reduction [66,67]. Because of these finalities, the study of dye-sensitized electrodes is usually aimed at the analysis of the light absorption properties and at the determination of the efficiency of photoelectrochemical conversion in the process of interest. In this context of research, a less considered (but not less important) aspect is represented by the analysis of the electrochemical properties of the electrode in the dye-sensitized state when the system is in dark conditions (i.e., the evaluation of the electrochemical properties of a photoelectrode in the "blank" state) [68]. In the particular case of dye-sensitized NiO for *p*-DSC purposes, the observation of a series of effects imparted by the dye sensitizer to the oxide substrate has been previously reported, even in absence of illumination [68–70]. These effects mostly consisted of the passivation of the NiO surface towards the oxidation of the NiO substrate itself [69–71], the observation of additional redox processes based on the immobilized dye (representing the actual redox-active species) [72], and redox processes following the synergy between the dye and oxide due to the spontaneous exchange of electronic charge between the dye and the oxide in the unbiased state [72]. The present contribution reports a study on the electrochemical and photoelectrochemical properties of NiO thin films prepared via screen printing [36,73,74] when the NiO electrode is either in the pristine state or in the dye-sensitized version. In particular, we considered the sensitization of nanostructured NiO with a series of organic dyes, the optical absorption properties of which span the visible and (near-infrared) NIR ranges. The structures of the nine dyes here employed as sensitizers of NiO are reported in the Supplementary Materials (Figures S1–S3). The colorants here considered are P1 [75–78], Fast Green (FG) [79,80], erythrosine B (ERY) [3,81–83], the series of the differently substituted squaraines DS_35, DS_44, and DS_46 [84,85], and the series of squaraines VG_1, VG_10, and VG_11, which differ to the extent of electronic conjugation [86].

2. Materials and Methods

Mesoporous NiO thin films have been deposited via screen printing of a paste containing NiO nanoparticles in accordance to the procedure reported in [36]. The scheme of preparation of the paste is reported in Table S1. The paste was successively screen printed onto Fluorine doped Tin Oxide (FTO)-coated glass and annealed at 450 °C in an oven, and a non-stoichiometric film of porous nickel oxide (l = 2.5 μm) was obtained [36]. The resulting film of NiO was nanostructured (Figure 1) and was used successively as a photocathode of a *p*-DSC in both pristine and sensitized states. The morphology of the NiO film is the same for all the employed cathodes as proved by SEM analyses. NiO was sensitized with the series of commercial dyes, P1, Erythrosine B (ERYB), and Fast Green (FG), and the series of squaraines prepared in laboratory scale, DS_35, DS_44, DS_46, VG_1, VG_10, and VG_11. The procedures of the syntheses of the six squaraines here considered have been reported elsewhere [87,88]. The sensitization procedure consisted of the dipping of the electrode in a solution of the given sensitizer. The solvent and the dipping time varied with regard to the colorant employed. When P1 was the sensitizer, the electrode was dipped in a 0.3 mM solution of P1 in acetonitrile for 16 h. The solutions of NiO sensitization with ERYB and FG had ethanol as the solvent, and for both dyes, the concentration was 0.3 mM [70,81,83,89]. The corresponding dipping time was 16 h. When the squaraine was employed, the sensitization was performed for 2 h in a 0.3 mM solution of each dye in ethanol. The shorter duration of the dipping time was used to avoid molecular aggregation [86].

Cyclic voltammetry (CV) measurements have been carried out in a three-electrodes cell. The potential was cyclically varied from open circuit voltage toward more cathodic potential to 1.2 V and further back to −0.27 V. More than 10 cycles have been recorded for each device in order to highlight any modification of the electrode behavior due to potential variation. The analyses of three different cells (sensitized with the same dye) led to identical results. Electrochemical impedance spectroscopy (EIS) measurements have been carried out in a three-electrodes configuration cell.

A constant perturbation of ±20 mV from open-circuit voltage has been supplied by a potentiostat (AUTOLAB PGSTAT12® from Metrohm, Herisau, Switzerland) during all the measurements, whereas the frequencies have been modulated from 100 KHz to 1 Hz: applied frequencies lower than 1 Hz led to unreliable (and non-reproducible) experimental points. Bode's plot was used to report the experimental data. In both CV and EIS experiments, the working electrode (WE) was a film of NiO deposited onto a FTO-coated glass, the counter electrode (CE) was a platinum rod, and the reference electrode was an Ag/AgCl electrode (+0.222 mV vs. NHE (Normal Hydrogen Electrode)). All the potentials reported throughout this work are referred to it. In all the experiments, the electrolyte solution was $LiClO_4$ 0.2 M in ACN (Acetonitrile). All figures have been plotted with the application Kaleidagraph 3.6, and their photoelectrochemical characterization has been already described in previous works [36,85,86].

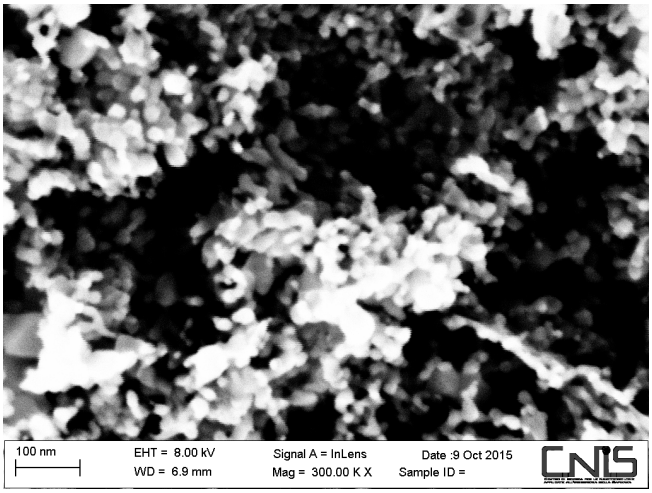

Figure 1. SEM picture of the mesoporous NiO film (thickness, l = 2 μm) here employed as the working electrode and dye-sensitized solar cells of *p*-type (*p*-DSC) photocathode.

3. Results and Discussion

3.1. Analysis of the Voltammetric Data

After sensitization of screen-printed NiO, the open-circuit voltage (V_{OC}) of the three-electrode cell with the dye-sensitized NiO as the working electrode was recorded. The corresponding values are displayed in Table 1.

The bare NiO in the native nanostructured version presents an excess of positive charge on its surface due to the presence of defective Ni(III) centers [26,91]. Such surface-localized species are responsible for the anchoring of the dye sensitizer [68] due to the hydrolysis reaction between the electron deficient site of Ni(III) and the carboxylic group of the colorant [92]. Such a process of sensitization diminishes the positive charge exposed to the electrolyte in passing from the sensitized NiO to the bare NiO with a consequent decrease of the potential difference across the double layer [71]. As a consequence of that, in dark conditions, the open-circuit voltage (OCV_{dark}) of the three-electrode cell with sensitized NiO as the working electrode will be lower with respect to the value displayed by the cell with the bare NiO electrode. All observed values of the OCV_{dark} for the three-electrode cells having sensitized NiO as the working electrode (WE) (see Table 1) are consistent with the given depiction of the mechanism of sensitization. Because dye anchoring is supposed to annihilate the positively charged sites on the surface of the defective nanostructured NiO, the extent of the OCV_{dark} decrease is related to the degree of surface passivation and, as a such, represents a measure of the efficacy with which a single molecule covers the NiO electrode surface. In fact, the combined analysis

of the dye loading and the OCV_{dark} data can be of some usefulness to estimate the apparent volume of a dye when in the surface-immobilized state [86].

Table 1. Second column from left: list of open-circuit potential values V_{OC} of the three-electrode cells differing for the nature of the sensitizer anchored on the NiO-working electrode. In the third column from left, the values of $V_{OC,20}$ refer to the open-circuit value of the cell after electrochemical cycling. The number of consecutive electrochemical cycles was 20 (*vide infra*). The given value was recorded when the open-circuit potential was steady for at least 30 min after the conduction of 20 voltammetric cycles within the potential range $-0.3\ V \leq E_{appl} \leq 1.2\ V$ vs. Ag/AgCl. The first column on the right lists the values of dye loading on the NiO film determined via the desorption method described in [90]. For the quantitative determination of dye loading in the case of the NiO sample sensitized with Fast Green (FG), the desorption method could not be adopted because of the scarce effect of dye desorption with the ordinary bleaching agents having medium basic strength.

Dye	V_{OC} (mV) vs. Ag/AgCl	Dye Loading (10^{-8} mol cm^{-2})
–	360	–
P1	140	20 [a]
FG	−55	NA
ERY	265	1.23
VG_1	150	1.63
VG_10	30	1.73
VG_11	120	2.35
DS44	130	1.12
DS35	120	0.87
DS46	85	0.35

[a] from ref. [55]. ERY: erythrosine B.

Within the family of DS squaraines, all three members possess the same extent of electronic conjugation but differ in the length of the alkyl chain [44]. Because the difference (OCV_{dark}(NiO) − OCV_{dark}(NiO-DS)) increases from DS_44 (230 mV) to DS_46 (275 mV), with DS_35 displaying the intermediate value (240 mV), we evince that DS_46, with its longer substituent (dodecyl group) and the lowest surface concentration (0.35×10^{-8} mol cm^2), is the sensitizer with the strongest ability to passivate the surface charge of NiO among the three symmetric squaraines of the DS family. In conclusion, the differences in the passivation action of the DS dyes reside mostly on the bulkiness of the substituent given the equality of extension of the conjugated skeleton (Figure S2). Therefore, after sensitization of NiO with DS squaraines, the alkyl chains also cover those electron-deficient sites of the surface, which have not been involved in the process of dye sensitization. In doing so, the alkyl chains of immobilized DS molecules prevent the further sensitization of the NiO surface despite the availability of free sites of anchoring. Within the group of VG squaraines, the structural differences among the three members consist of the enlargement of the structure in passing from VG_1 to VG_10 and VG_11 due to the additional presence of a condensed additional phenyl ring in VG_10 and VG_11. Such a variation brings about an extension of the conjugated moiety in VG_10 and VG_11 in comparison to VG_1, with consequences on the main property of the electronic polarizability. Data in Table 1 show that VG_1-sensitized NiO produces the cell with the highest value of OCV_{dark}(NiO) within the group of VG dyes. Such a finding is consistent with the previous considerations of the factors controlling the passivating effect of a dye when in the anchored state: VG_1 represents the dye with the smallest volume with respect to VG_10 and VG_11 due to the lack of two condensed benzene rings (Figure S3). For this reason, the passivation of the excess charge on the NiO surface with VG_1 will be less efficacious in comparison with VG_10 and VG_11, and the corresponding value of OCV_{dark}(VG_1-NiO) will be larger (150 mV) than OCV_{dark}(VG_10-NiO) and OCV_{dark}(VG_11-NiO) with 30 and 120 mV, respectively (Table 1). When the OCV_{dark} values of the cells with VG_10- and VG_11-sensitized NiO WEs are compared, a strong diminution of OCV_{dark} is observed from VG_11 to VG_10 (120 mV vs. 30 mV, Table 1). Accordingly, two important points have to be evidenced

when VG_10 and VG_11 are confronted: (1) the presence of two strong electron-withdrawing groups in VG_1 (i.e., the cyano groups) which replace an atom of oxygen in the four terms ring; (2) a minor conformational freedom of VG_11 versus VG_10 due to the limitation of the rotation of the benzo-isoindoline moieties around the bond that links them to the squaric ring as imposed by the presence of the bulkier cyano groups in VG_11. The remarkably low value of OCV_{dark}(VG_10-NiO) within the VG series could be due to the concomitant action of several factors: (a) enhanced electron donor properties of the benzo-isoindoline moiety towards the electron-deficient sites of NiO with respect to the isoindoline unit of VG_1; (b) despite the analogous extension of the electronically conjugated network, VG_10 lacks two CN groups (i.e., electron-withdrawing groups), which disfavor the retro-donation of negative charge from the dye molecule to the positive centers localized on the NiO surface when VG_11 is the sensitizer. For this reason, it is expected to observe a larger diminution of OCV_{dark} with respect to the bare NiO in passing from the cell with a VG_10-sensitized electrode to the one with a VG_11-sensitizer. In other words, VG_10 compensates more efficiently the electron deficiency of the NiO surface by virtue of its more favorable properties of electron donation with respect to VG_1 and VG_11. A comparison of the trends of OCV_{dark} values for the VG and DS families of squaraines is rendered quite complicated by the differences in the number of anchoring groups (four in DSs and two in VGs), the extension of the conjugated moiety, and the presence of the amino-phenyl moiety in sole DSs. For this reason, we do not attempt an explanation of the differences in the OCV_{dark} values for the groups of VGs and DSs. A similar shift of open-circuit potential is also observed when screen-printed NiO film is sensitized with coumarin 153 and coumarin 343 (see Table S2 and Figure S4 in the Supplementary Materials). When NiO is electrochemically cycled in non-aqueous solvent within the potential range in which the oxide undergoes the series of solid state oxidation processes [27], the following occurs:

$$NiO + m{ClO_4}^- \rightarrow Ni(II)_{1-m}ONi(III)_m(ClO_4)_m + me^- \quad (1)$$

$$Ni(II)_{1-m}ONi(III)_m(ClO_4)_m + m{ClO_4}^- \rightarrow Ni(II)_{1-m}ONi(IV)_m(ClO_4)_{2m} + me^- \quad (2)$$

Two broad peaks appear in the relative voltammogram of NiO (black trace in Figure 2 and Figure S5 in the Supplementary Materials). The oxidation peak observed at the lower applied potential corresponds to the process of Equation (1), whereas the oxidation occurring at the higher potential refers to the redox process of Equation (2) [3].

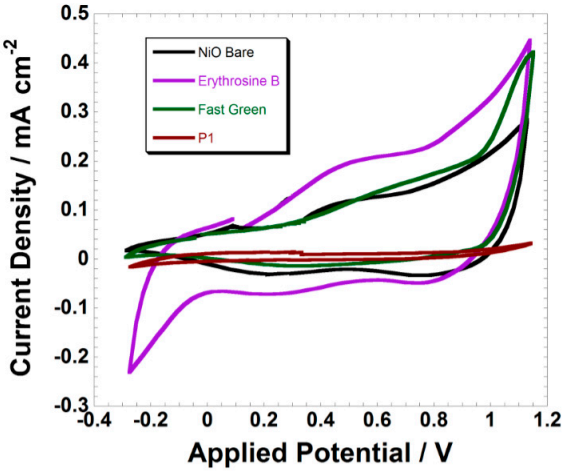

Figure 2. Variation of the voltammogram of screen-printed NiO electrodes in passing from the bare state (black trace) to the sensitized ones with ERY, FG, and P1 (see Figure S1 for the corresponding structures). Scan rate: 100 mV s^{-1}.

The adoption of P1 as a sensitizing agent has a clear effect of NiO surface passivation towards the redox processes of Equations (1) and (2) (brown-reddish trace in Figure 2) in accordance to previously reported data, which referred to the P1-sensitized NiO electrodes deposited via rapid discharge sintering (RDS) [75]. This is not the case of ERY-sensitized NiO (violet trace in Figure 2), because the presence of the sensitizer amplifies the current wave associated with the oxidation of NiO with respect to the electrochemical response of the bare oxide (black trace in Figure 2). Moreover, the NiO electrode sensitized with ERY does not display any additional redox peak or a potential shift of the oxidation peaks with respect to pristine NiO. This combination of findings evidences that the ERY sensitizer does not alter the nature of the redox processes NiO undergoes (Equations (1) and (2)). The verification of a decrease of the open-circuit potential going from the bare NiO to the ERY-sensitized version indicates that ERY mainly acts as an electron-donor towards NiO with consequent increases of the number of surface sites prone to electrochemical oxidation. Thus, a process of the following type can be predicted:

$$h^{+}_{(NiO)} + ERY \rightarrow [e^{-}\text{-}h^{+}]_{(NiO)} + (ERY)^{+} \quad (3)$$

where the holes $h^{+}_{(NiO)}$ localized on the NiO surface represent the defective Ni(III) sites of the pristine oxide [23,26]. This is equivalent to say that chemisorbed ERY induces the chemical conversion Ni(III) → Ni(II). As a consequence of that, an increase in the oxidative current associated with the process of Equation (1) should be expected. In some precedent cases, it has been also verified that ERY exerts a passivating action on the surface of (Rapid Discharge Sintering) RDS-NiO [83] similar to what we have observed here with P1 (brown-reddish trace in Figure 2). Such discrepant behaviors of ERY as a NiO sensitizer have to be ascribed to the differences in the surface compositions of the differently prepared NiO samples. In fact, the extent of the charge transfer from ERY to NiO depends on several characteristics of the NiO substrate, such as the surface concentration of defective Ni(III) sites, surface concentration of the sites of dye anchoring (such "species" do not necessarily coincide with the defective Ni(III) centers) [86], degree of NiO surface hydration [26], porosity [55], and extent of dye coverage.

The FG sensitizer shows an apparent effect of NiO surface passivation (green trace in Figure 2 and brown-reddish trace in the left frame of Figure 3) as far as the process of NiO oxidation at lower potential is concerned (Equation (1)). Moreover, FG introduces an additional peak of oxidation due to the electroactivity of the dye itself (see the comparison of the two traces in the left frame of Figure 3).

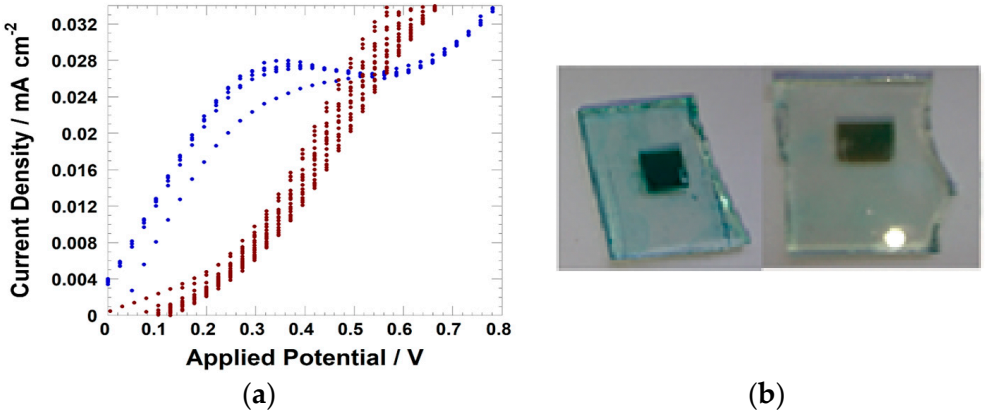

Figure 3. (**a**) Zooming of the voltammograms of the bare NiO (blue trace) and FG-sensitized NiO (brown-reddish dots); (**b**) Photograph of FG-sensitized NiO prior the treatment of electrochemical cycling (colored sample on the left) and after electrochemical cycling (bleached sample on the right).

The peak of FG oxidation overlaps with the oxidation process of NiO reported in Equation (2). After one cycle, the NiO electrode became decolored (photograph in the right frame of Figure 3). The oxidation of immobilized FG then brings about the detachment of the dye from the surface of

NiO. This effect is probably due to the scarce electrochemical stability of the sulfonic group as a linker of FG [92]. DS squaraines in the immobilized state have also shown an analogous behavior upon continuous electrochemical cycling (Figure 4) [72].

The first cycle of DS_46-sensitized NiO in Figure 4 is characterized by the presence of two irreversible current peaks (Figure 4a) that do not appear in the successive scans (Figure 4b). We attribute this sequence of events to the combined oxidation of DS_46 and NiO during the first cycle with successive peeling-off of the dye from the substrate. In the first cycle, the process of NiO oxidation (Figures 2 and S5) is completely masked by the much ampler wave of current associated with DS_46 oxidation. The amplitude of the oxidation peaks of DS_46 is ca. 10 times larger than the amplitude of the peaks characteristic of NiO oxidation. In the successive cycles, the current peaks we attributed to the oxidation of DS_46 were no longer present. Moreover, the voltammograms of the successive cycles recall the ones of the bare NiO within the same potential range (comparison between the voltammetric profiles in the left frame of Figure 4 and the black trace of Figure 2). The hypothesis of the detachment of DS_46 consequent to its surface oxidation is supported by the observation of electrode decoloration after the treatment of electrochemical cycling (Figures 5 and S6). An analogous electrochemical behavior has been observed when screen-printed NiO was sensitized with the other squaraines DS_35, DS_44, VG_1, VG_10, and VG_11 (see Figures S7–S11 in the Supplementary Materials). The electrochemical behavior of the screen-printed NiO sensitized with the series of squaraines considered here is consistent with the findings reported in previous works about the electrochemical and photoelectrochemical properties of various NiO samples sensitized with the commercial squaraine SQ2 [72,93,94].

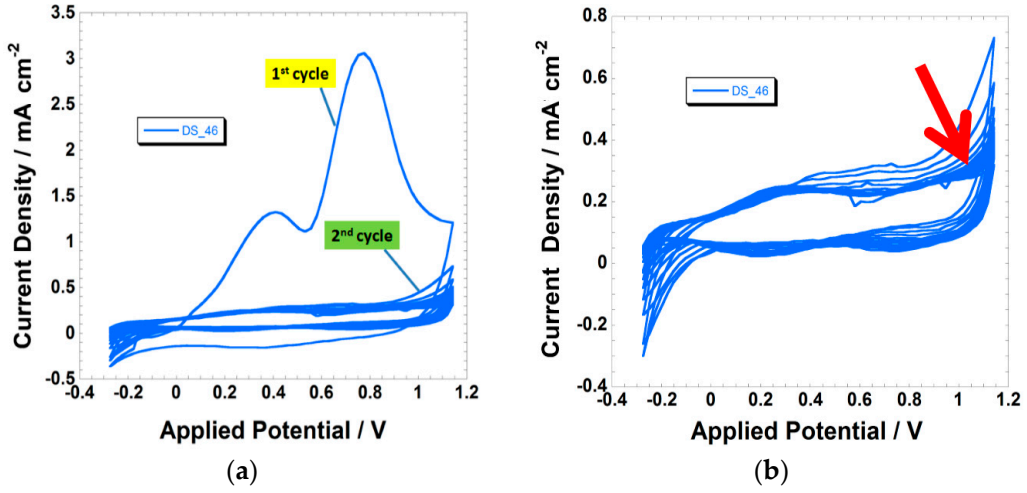

Figure 4. (**a**) First 20 voltammograms of the DS_46-sensitized NiO electrode at the scan rate of 100 mV s^{-1}. The first two cycles are indicated; (**b**) Stabilization of the voltammogram of the DS_46-sensitized electrode after the first cycle, evidenced in the left frame. The red arrow indicates the sense of variation of the current profile upon the increase of the number of cycles. See Figure S2 for the visualization of the dye structure.

The voltammograms of coumarin-sensitized NiO electrodes are shown in Figure S12 (see Supplementary Materials). Different from squaraines, surface-immobilized coumarins do not introduce redox peaks associated with the redox activity of the dye. Moreover, the observation of a scarce effect of NiO surface passivation, as well as a poor effect of NiO sensitization indicate that coumarins do not anchor in large amounts onto the mesoporous NiO surface prepared via screen printing.

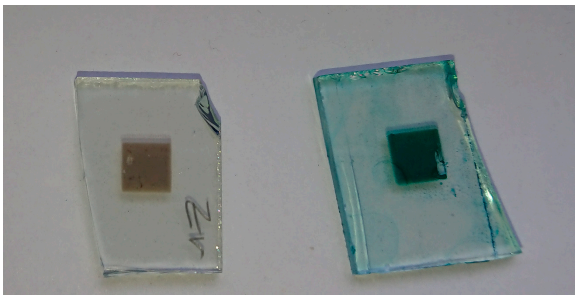

(**a**) (**b**)

Figure 5. Photographs of DS_46-sensitized NiO film before (**a**) and after (**b**) the electrochemical cycling of Figure 4.

3.2. Analysis of the Impedance Spectra

The electrochemical impedance spectra of the three-electrode cells having the bare or sensitized NiO as the working electrode have been recorded at open-circuit potential (V_{OC}). The corresponding values of V_{OC} for the cells with differently sensitized NiO electrodes are those reported in the second column of Table 1 (*vide supra*). After the assembly of the cell, its value of V_{OC} was first measured. The impedance spectrum of the cell was recorded immediately after the determination of V_{OC} with the cell potential kept at the given value of V_{OC}.

The impedance analysis was not conducted on the cells after the treatment of electrochemical cycling, because it has been observed that electrochemical cycling generally introduces irreversible modifications of the sensitized electrode (i.e., partial or complete desorption of the dye). It is worth mentioning that the electrochemical cycling did not provoke any structural modification in the electrode. To confirm that, we reported some SEM images (see Figure S6 Page: 8 and Table S3) of pristine NiO, sensitized NiO, and cycled-sensitized NiO. No meaningful structural variations may be highlighted. Interestingly, EDX (Energy Dispersion X-ray) analyses showed different elemental distributions for the three electrodes: compared to the bare NiO, the sensitized electrode has a higher carbon content due to the organic molecule chemisorbed onto the NiO surface. After cycling, the carbon content decreases, but it is still higher compared to the pristine electrode. The latter evidence is consistent with the dye degradation evidenced during the CV experiments: the sensitizer occurred in some oxidation reactions (and it did not still adsorb visible light), but it did not completely detach from NiO, and it partially contributes to the electrode passivation (see above). As previously shown, dye desorption/degradation has been verified through the continuous changes of the shape of the voltammograms with cycling (Figure 4 and Figures S7–S12 in the Supplementary Materials) and through the non-negligible variation of the open-circuit potential of the cell in passing from the pristine state to the cycled one (V_{OC} vs. $V_{OC,20}$ in Table 1). Figures 6–8 present the impedance spectra of the differently sensitized cells in the form of Bode plots.

The impedance data presented in Figures 6–8 were fitted with the response calculated for the equivalent circuits displayed in Figures 9 and 10. Two distinct models were considered depending on the eventual presence of the dye sensitizer on the electrode surface. The model of Figure 9 is characterized by the parallel connection of the charge transfer resistance through the bare electrode/electrolyte interface ($R_{NiO/el}$) to the capacitive element $CPE_{NiO/el}$. The latter circuital element is associated with the charge distribution representing the electrochemical double layer at the bare NiO/electrolyte interface. The second model of equivalent circuit (Figure 10) accounts for the presence of the immobilized sensitizer and considers accordingly the additional interface NiO/dye created by the combination of the electrode with the dye sensitizer. The consideration of the NiO/dye interface as the relevant electrical element of the modified electrode has led to the insertion of the parallel terms R_{ct} (=resistance of the charge transfer between NiO substrate and dye) and CPE_{ct} (=element of constant phase, which refers to the charge distribution at the NiO/dye interface during the charge transfer)

in the model of Figure 10. The fit of the impedance spectrum of the cell with the bare NiO as the working electrode was realized when $R_{NiO/el}$ = 4517 ± 53 Ω and the double-layer capacitance at the NiO/electrolyte interface $C_{NiO/el}$ was 8.06 ± 0.80 μF. Table 2 lists the fitting values of the electrical parameters $R_{NiO\text{-}D/el}$, R_{ct} (Figure 10) and $C_{NiO\text{-}D/el}$. The latter capacitive element refers to the charge distribution at the interface formed by the sensitized NiO electrode in contact with the electrolyte. The simulated impedance spectra are shown in the Supplementary Materials (Figures S13–S22).

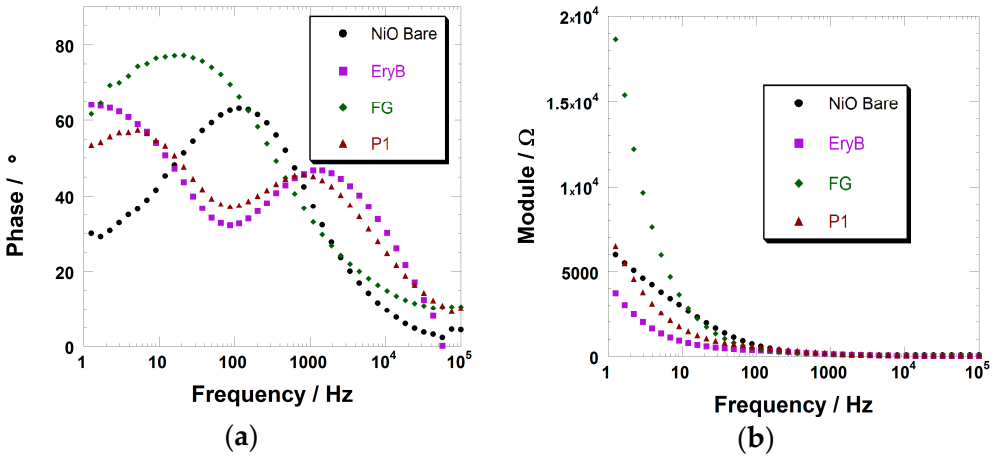

Figure 6. (**a**) Variation of the phase of the electrochemical impedance with the frequency of the potential stimulus for the cells with the bare, ERY-, P1-, and FG-sensitized NiO as the working electrode; (**b**) Variation of the impedance modulus with the frequency of stimulus for the four cells analyzed in the left frame.

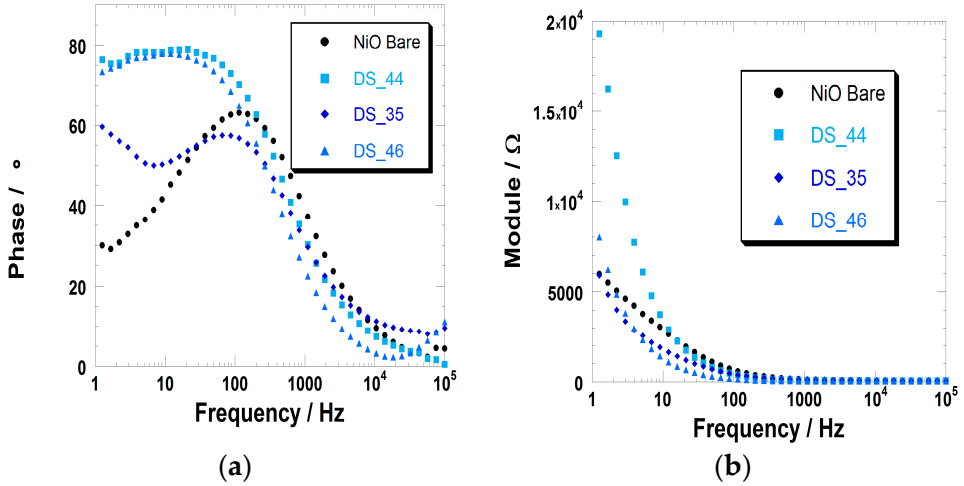

Figure 7. (**a**) Variation of the phase of the electrochemical impedance with the frequency of the potential stimulus for the cells with the bare, DS_35-, DS_44-, and DS_46-sensitized NiO as the working electrode; (**b**) Variation of the impedance modulus with the frequency of stimulus for the four cells analyzed in the left frame.

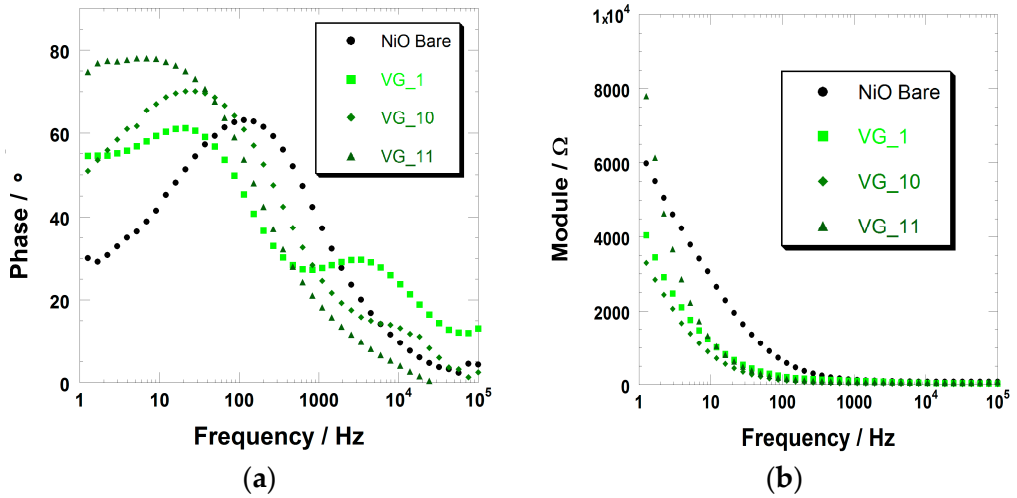

Figure 8. (**a**) Variation of the phase of the electrochemical impedance with the frequency of the potential stimulus for the cells with bare, VG_1-, VG_10-, and VG_11-sensitized NiO as the working electrode. (**b**) Variation of the impedance modulus with the frequency of stimulus for the four cells analyzed in the left frame.

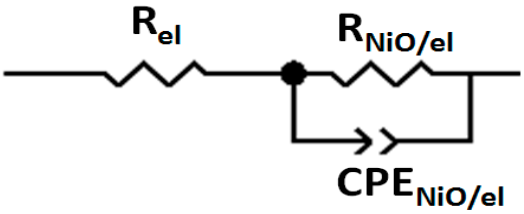

Figure 9. Model of equivalent circuit for the fitting of the electrochemical impedance spectroscopy (EIS) data recorded at the potential of the open circuit of three-electrode cell with the bare NiO as the working electrode. R_{el}: the sum of all the resistances due to the circuital elements except the working electrode. $R_{NiO/el}$: resistance of the charge transfer through the interface created by the bare NiO and the electrolyte; $CPE_{NiO/el}$: element of the constant phase, which refers to the charge distribution during the process of the charge transfer through the interface created by the bare NiO and the electrolyte.

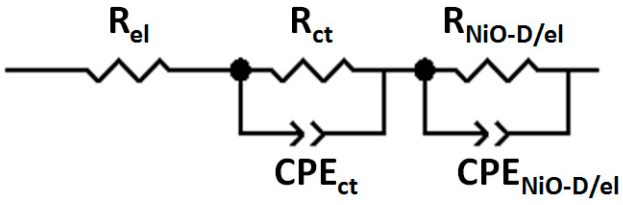

Figure 10. Model of the equivalent circuit for the fitting of the EIS data recorded at the potential of open circuit of three-electrode cell with dye-sensitized NiO as the working electrode. R_{el}: the sum of all the resistances due to the circuital elements except the working electrode; R_{ct}: resistance of the charge transfer between the NiO substrate and the dye; CPE_{ct}: element of the constant phase, which refers to the charge distribution at the NiO/dye interface during the process of the charge transfer between the NiO and the dye; $R_{NiO-D/el}$: resistance of the charge transfer through the interface created by the sensitized electrode and electrolyte; $CPE_{NiO-D/el}$: element of the constant phase, which refers to the charge distribution during the process of the charge transfer through the interface created by the sensitized electrode and the electrolyte.

In the Bode's plot, phase diagrams usually exhibit a number of peaks corresponding to the number of RC (Resistor-Capacitor) elements. This is true when investigated phenomena occur in different time scales. In the present case, this happened for just some of the sensitized electrodes (e.g., P1, ERYB, and VG_11). When FG or the dyes from the DS series are employed as the sensitizer, the two phenomena (i.e., the charge transfer from the NiO to the dye and the charge transfer from the sensitized electrode to the electrolyte) occurs in a quite similar time scale, and the two peaks tend to merge into (a broadened) one, straightforwardly. It is worth mentioning that a different time scale between the two reactions is typical of well-performing sensitizers (see Table 3 below).

Impedance data confirm that the dye sensitizer generally acts as a passivating agent of the NiO surface, because the resistance of the charge transfer through the electrode/electrolyte interface is systematically higher for the sensitized electrode ($R_{\text{NiO-D/el}} > 14$ kΩ, Table 2, second column from left) with respect to the pristine NiO ($R_{\text{NiO/el}} < 5$ kΩ). Because the characteristic electrochemical processes of NiO consist of the simultaneous injection of the electronic charges and ion uptake (Equations (1) and (2)), the presence of the dye sensitizer with its steric hindrance impedes the approach of the charge, compensating ions towards the surface of NiO during its oxidation. As a confirmation of that, the largest values of the charge transfer resistance are found when the NiO is sensitized by the dyes with the largest skeleton or the longer pending groups within the same series. These are the cases of VG_11 within the VG series (Figure S3) and of DS_46 within the DS series (Figure S2).

Table 2. List of the fitting values of $R_{\text{NiO-D/el}}$, R_{ct}, and $C_{\text{NiO-D/el}}$ for the simulation of the impedance spectra of the cells with sensitized NiO electrodes at the condition of open-circuit potential. The meaning of the terms $R_{\text{NiO-D/el}}$ and R_{ct} is the same as reported in the caption of Figure 10. $C_{\text{NiO-D/el}}$ is the capacitance of the double layer at the sensitized NiO/electrolyte interface.

Dye	$R_{\text{NiO-D/el}}$ (Ω)	R_{ct} (Ω)	$C_{\text{NiO-D/el}}$ (μF)	R_{rec} (Ω)
P1	58,212 ± 456	292.6 ± 2.9	6.52 ± 0.70	85.2
ERY	23,611 ± 221	455.5 ± 4.9	8.62 ± 0.69	63.1
FG	37,938 ± 412	4023 ± 53	6.91 ± 0.76	58.6
DS_44	15,230 ± 144	1328 ± 18	6.72 ± 0.86	52.3
DS_35	29,035 ± 258	2899 ± 36	7.66 ± 0.68	72.9
DS_46	69,673 ± 665	3204 ± 39	7.97 ± 0.76	96.7
VG_1	14,447 ± 153	602.3 ± 10.3	6.08 ± 1.16	15.8
VG_10	22,059 ± 196	424.2 ± 12.0	6.30 ± 1.15	60.3
VG_11	71,463 ± 423	187.9 ± 2.3	8.59 ± 0.68	71.5

Analogous considerations hold when the resistances of FG- and P1-sensitized NiO electrodes are compared to that of ERY-sensitized NiO (Figure S1). Dye loading (Table 1, first column from the right) does not appear as crucial as the size of the dye in controlling the interfacial resistance $R_{\text{NiO-D/el}}$. This is probably because the variations of dye loading are not large enough to generate substantial differences of passivating action within the set of dye sensitizers here considered. With the exception of NiO sensitization with ERY and VG_11, dye chemisorption generally leads to a decrease of the double-layer capacitance of the electrode/electrolyte interface $C_{\text{NiO-D/el}}$ with respect to the bare NiO. Such a diminution of $C_{\text{NiO-D/el}}$ is consistent with the effect of masking of the NiO surface charge, which is produced by the sensitizer as previously discussed during the analysis of the trend of V_{OC} (Table 1).

The dark resistance of the charge transfer between the NiO substrate and the dye sensitizer (the R_{ct} term defined in Figure 10) refers to the process of the charge injection in the NiO with the dye in the ground state, which acts as mediator. We show here that such a resistive term (that is determined in the absence of illumination in a three-electrode cell with a dye-sensitized working electrode) can represent a valid parameter for the evaluation of the efficacy with which the dye in the optically excited state transfers electronic charge to the semiconducting substrate during the operation of an illuminated dye-sensitized solar cell [95]. Table 3 reports the fundamental photoelectrochemical parameters of

the *p*-DSCs, employing the same dye-sensitized electrodes of the experiments shown in Figures 6–8 when the redox shuttle is the couple I^-/I_3^- and the counter electrode is platinized FTO. R_{rec} is the recombination resistance at the NiO/electrolyte interface in complete device configuration.

It is found that the sensitizers producing the largest efficiencies of conversion η (>0.030%, Table 3) in the corresponding *p*-DSCs employing the NiO cathodes display generally the lowest values of the dark parameter R_{CT} within the same series of compounds. This is particularly evident in the cases of P1 and ERY and in the cases of the DS_44 and VG_11 sensitizers within their respective families of squaraines. The existence of a correlation between the trends of η and R_{CT} within the same class of compounds indicates that when the electron transfer (*et*) between the NiO and the ground state of the sensitizer is efficient, the process of *et* between the NiO substrate and the excited state of the sensitizer is as efficient as the one conducted in dark conditions, despite the involvement of different electronic states of the sensitizer (and probably of different energy levels in the electronic structure of the mesoporous, semiconducting NiO) [96] in these two processes.

Table 3. Values of the relevant parameters' open-circuit photopotential (V_{OC}), short-circuit current density (J_{SC}), fill factor (FF), and overall conversion efficiency (η), which characterize the photoelectrochemical performance of a *p*-DSC with a sensitized NiO photocathode. For the assembly of the DSC and the determination of the photoelectrochemical parameters, we adopted the experimental conditions reported in [97]. Data of the *p*-DSCs employing FG-sensitized NiO photocathodes could not be determined for the scarce time stability of the relative photoelectrochemical response.

Dye	V_{OC} (mV)	J_{SC} (mA cm^{-2})	FF (%)	η (%)	Ref.
–	96	−0.261	40.76	0.01	–
ERY	88	−1.019	36.02	0.032	[86]
P1	125.6	−1.188	32.9	0.049	–
VG_1	87	−0.577	37.2	0.018	[86]
VG_10	102	−0.435	40.87	0.018	[86]
VG_11	93	−1.16	36.12	0.043	[86]
DS_44	101	−0.991	37.12	0.037	[85]
DS_35	95	−0.821	37.94	0.03	[85]
DS_46	94	−0.503	36.46	0.017	[85]

4. Conclusions

In the present work, the electrochemical characterization of screen-printed NiO electrodes sensitized with the commercial benchmarks ERY, P1, and FG and with two series of squaraines, differing according to the extent of electronic conjugation (VG series) and the size of peripheral substituents (DS series), has been considered. The presence of the chemisorbed sensitizers P1 and FG on the screen-printed NiO induces an effect of passivation of the oxide surface against NiO oxidation. Such an effect manifests itself through the decrease of the intensity of the characteristic peaks of NiO oxidation when the oxide passes from the bare to the P1- or FG-sensitized state. In such cases, the electronic interactions between the dye sensitizer and the NiO surface can be considered weak, because no process of charge transfer between the dye and the oxide occurs in dark conditions or for small polarizations of the sensitized NiO electrode. Squaraines and, to a lesser extent, FG undergo a process of electrochemical oxidation in the immobilized state when the applied potential falls in the range of NiO electroactivity. Such a redox process brings about the disruption of the electronic conjugation in the dye skeleton and its successive detachment from the substrate. This was verified by the decoloration of the electrochemically cycled NiO. Because the solid-state electrochemical process of NiO oxidation consists of the dark injection of holes (i.e., the formation of Ni(III) centers, which render nickel oxide a non-stoichiometric system), such a finding warns us about the employment of squaraines (and FG) as dye sensitizers of NiO in *p*-type dye-sensitized solar cells: their use must be particularly judicious. The occurrence of the oxidation for NiO and squaraines within the same range of applied potential indicated that the simultaneous presence of holes in the NiO and the oxidized dye in the immobilized

state is deleterious for the chemical stability of the linker anchoring the dye to the NiO surface. Consequently, the diffusion of the photoinjected holes towards the NiO bulk has to occur faster than the onset of the degrading process of linker rupture, which starts from the excess of positive charge at the dye/electrode junction. Different to all other sensitizers here examined, ERY produced the opposite effect of dark current enhancement corresponding with the electrochemical oxidation processes of NiO. Such a finding has been attributed to the occurrence of a spontaneous process of electron transfer from the ERY sensitizer to the defective Ni(III) centers of the NiO surface in the absence of any external polarization. The consequence of the resulting conversion Ni(III) → Ni(II) would be the increase of the surface sites of NiO, which undergo electrochemical oxidation. The electrochemical impedance spectra of the differently sensitized electrodes have been analyzed and modeled with two distinct equivalent circuits depending on the version of the NiO electrode (i.e., pristine or sensitized). Within a set of dye, we could find a correlation between the trend of the dark charge transfer resistance at the electrode/dye junction and the trend of the overall efficiency of photoconversion in the corresponding dye-sensitized solar cells employing the same sensitized electrode as a photocathode. The photoelectrochemical cells displaying the highest efficiencies of solar conversion were those that employed sensitized NiO electrodes with the lowest values of charge transfer resistance through the dye/NiO junction in the absence of illumination. This finding would indicate that the electronic communication between the NiO substrate and the dye sensitizer is the most important factor of control of the electrochemical and photoelectrochemical processes occurring at this type of modified semiconductor.

Supplementary Materials: The following are available online at http://www.mdpi.com/2079-6412/8/7/232/s1, Figure S1: Structure of the commercial dyes, Figure S2: Structure of the squaraines (DS-series), Figure S3: Structure of the squaraines (VG-series), Figure S4: Structures of coumarin dyes, Figure S5: Voltammogram of bare NiO, Figure S6: SEM images of different electrodes, Figure S7–S12: CV curves, Figure S13–S22: Bode plots; Table S1: Procedure of the preparation of the paste P3, Table S2: Variation of VOC for the cells with coumarin-sensitized NiO, Table S3: EDX elemental analyses.

Author Contributions: Conceptualization, Danilo Dini and Matteo Bonomo; Methodology, All Authors; Validation, Danilo Dini, Matteo Bonomo and Claudia Barolo; Formal Analysis, Daniele Gatti and Matteo Bonomo; Investigation, Daniele Gatti and Matteo Bonomo; Resources, Matteo Bonomo and Claudia Barolo; Data Curation, Matteo Bonomo and Daniele Gatti; Writing-Original Draft Preparation, Matteo Bonomo and Danilo Dini; Writing-Review & Editing, Matteo Bonomo and Danilo Dini; Supervision, Danilo Dini, Matteo Bonomo and Claudia Barolo; Project Administration, Danilo Dini and Claudia Barolo.

Funding: This research received no external funding.

Conflicts of Interest: The authors declare no conflict of interest.

References

1. Passerini, S.; Scrosati, B. Characterization of Nonstoichiometric Nickel Oxide Thin-Film Electrodes. *J. Electrochem. Soc.* **1994**, *141*, 889–895. [CrossRef]
2. Wei, L.; Jiang, L.; Yuan, S.; Ren, X.; Zhao, Y.; Wang, Z.; Zhang, M.; Shi, L.; Li, D. Valence Band Edge Shifts and Charge-transfer Dynamics in Li-Doped NiO Based p-type DSSCs. *Electrochim. Acta* **2016**, *188*, 309–316. [CrossRef]
3. He, J.; Lindström, H.; Hagfeldt, A.; Lindquist, S.-E. Dye-Sensitized Nanostructured p-Type Nickel Oxide Film as a Photocathode for a Solar Cell. *J. Phys. Chem. B* **1999**, *103*, 8940–8943. [CrossRef]
4. Sahara, G.; Abe, R.; Higashi, M.; Morikawa, T.; Maeda, K.; Ueda, Y.; Ishitani, O. Photoelectrochemical CO_2 reduction using a Ru(II)-Re(I) multinuclear metal complex on a p-type semiconducting NiO electrode. *Chem. Commun.* **2015**, *51*, 10722–10725. [CrossRef] [PubMed]
5. Gross, M.A.; Creissen, C.E.; Orchard, K.L.; Reisner, E. Photoelectrochemical hydrogen production in water using a layer-by-layer assembly of a Ru dye and Ni catalyst on NiO. *Chem. Sci.* **2016**, *7*, 5537–5546. [CrossRef]
6. Dini, D. Nanostructured Metal Oxide Thin Films as Photoactive Cathodes of p-Type Dye-Sensitised Solar Cells. *Phys. Chem. Commun.* **2016**, *3*, 14–51.
7. Shan, B.; Sherman, B.D.; Klug, C.M.; Nayak, A.; Marquard, S.L.; Liu, Q.; Bullock, R.M.; Meyer, T.J. Modulating Hole Transport in Multilayered Photocathodes with Derivatized p-Type Nickel Oxide and Molecular Assemblies for Solar-Driven Water Splitting. *J. Phys. Chem. Lett.* **2017**, 4374–4379. [CrossRef] [PubMed]

8. Li, L.; Dai, H.; Luo, D.; Wang, S.; Sun, X. Nickel Oxide Nanosheets for Enhanced Photoelectrochemical Water Splitting by Hematite (α-Fe_2O_3) Nanowire Arrays. *Energy Technol.* **2016**, *639798*, 758–763. [CrossRef]
9. Yao, K.; Li, F.; He, Q.; Wang, X.; Jiang, Y.; Huang, H.; Jen, A.K.Y. A copper-doped nickel oxide bilayer for enhancing efficiency and stability of hysteresis-free inverted mesoporous perovskite solar cells. *Nano Energy* **2017**, *40*, 155–162. [CrossRef]
10. Mihelčič, M.; Šurca Vuk, A.; Jerman, I.; Orel, B.; Švegl, F.; Moulki, H.; Faure, C.; Campet, G.; Rougier, A. Comparison of electrochromic properties of $Ni_{1-x}O$ in lithium and lithium-free aprotic electrolytes: From $Ni_{1-x}O$ pigment coatings to flexible electrochromic devices. *Sol. Energy Mater. Sol. Cells* **2014**, *120*, 116–130. [CrossRef]
11. Da Rocha, M.; Rougier, A. Electrochromism of non-stoichiometric NiO thin film: As single layer and in full device. *Appl. Phys. A Mater. Sci. Process.* **2016**, *122*. [CrossRef]
12. Wen, R.T.; Granqvist, C.G.; Niklasson, G.A. Anodic electrochromism for energy-efficient windows: Cation/anion-based surface processes and effects of crystal facets in nickel oxide thin films. *Adv. Funct. Mater.* **2015**, *25*, 3359–3370. [CrossRef]
13. Zhao, C.C.; Chen, C.; Du, F.L.; Wang, J.M. Template synthesis of NiO ultrathin nanosheets using polystyrene nanospheres and their electrochromic properties. *RSC Adv.* **2015**, *5*, 38533–38537. [CrossRef]
14. Estrada, W.; Andersson, A.M.; Granqvist, C.G.; Gorenstein, A.; Decker, F. Infrared reflectance spectroscopy of electrochromic NiO_xH_y films made by reactive DC sputtering. *J. Mater. Res.* **1991**, *6*, 1715–1719. [CrossRef]
15. Choi, S.H.; Kang, Y.C. Ultrafast synthesis of yolk-shell and cubic NiO nanopowders and application in lithium ion batteries. *ACS Appl. Mater. Interfaces* **2014**, *6*, 2312–2316. [CrossRef] [PubMed]
16. Gu, L.; Xie, W.; Bai, S.; Liu, B.; Xue, S.; Li, Q.; He, D. Facile fabrication of binder-free NiO electrodes with high rate capacity for lithium-ion batteries. *Appl. Surf. Sci.* **2016**, *368*, 298–302. [CrossRef]
17. Yue, G.H.; Zhao, Y.C.; Wang, C.G.; Zhang, X.X.; Zhang, X.Q.; Xie, Q.S. Flower-like nickel oxide nanocomposites anode materials for excellent performance lithium-ion batteries. *Electrochim. Acta* **2015**, *152*, 315–322. [CrossRef]
18. Wang, C.; Wang, T.; Wang, B.; Zhou, X.; Cheng, X.; Sun, P.; Zheng, J.; Lu, G. Design of α-Fe_2O_3 nanorods functionalized tubular NiO nanostructure for discriminating toluene molecules. *Sci. Rep.* **2016**, *6*, 26432. [CrossRef] [PubMed]
19. Wang, C.; Cui, X.; Liu, J.; Zhou, X.; Cheng, X.; Sun, P.; Hu, X.; Li, X.; Zheng, J.; Lu, G. Design of Superior Ethanol Gas Sensor Based on Al-Doped NiO Nanorod-Flowers. *ACS Sens.* **2016**, *1*, 131–136. [CrossRef]
20. Bai, G.; Dai, H.; Deng, J.; Liu, Y.; Ji, K. Porous NiO nanoflowers and nanourchins: Highly active catalysts for toluene combustion. *Catal. Commun.* **2012**, *27*, 148–153. [CrossRef]
21. Yang, J.; Lai, Y.; Chen, J.S. Effect of heat treatment on the properties of non-stoichiometric p-type nickel oxide films deposited by reactive sputtering. *Thin Solid Films* **2005**, *488*, 242–246. [CrossRef]
22. Cavallo, C.; Di Pascasio, F.; Latini, A.; Bonomo, M.; Dini, D. Nanostructured Semiconductor Materials for Dye-Sensitized Solar Cells. *J. Nanomater.* **2017**, *2017*, 5323164. [CrossRef]
23. D'Amario, L.; Jiang, R.; Cappel, U.B.; Gibson, E.A.; Boschloo, G.; Rensmo, H.; Sun, L.; Hammarström, L.; Tian, H. Chemical and Physical Reduction of High Valence Ni States in Mesoporous NiO Film for Solar Cell Application. *ACS Appl. Mater. Interfaces* **2017**, *9*, 33470–33477. [CrossRef] [PubMed]
24. Boschloo, G.; Hagfeldt, A. Characteristics of the iodide/triiodide redox mediator in dye-sensitized solar cells. *Acc. Chem. Res.* **2009**, *42*, 1819–1826. [CrossRef] [PubMed]
25. Awais, M.; Dini, D.; Don MacElroy, J.M.; Halpin, Y.; Vos, J.G.; Dowling, D.P. Electrochemical characterization of NiO electrodes deposited via a scalable powder microblasting technique. *J. Electroanal. Chem.* **2013**, *689*, 185–192. [CrossRef]
26. Marrani, A.G.; Novelli, V.; Sheehan, S.; Dowling, D.P.; Dini, D. Probing the redox states at the surface of electroactive nanoporous nio thin films. *ACS Appl. Mater. Interfaces* **2014**, *6*, 143–152. [CrossRef] [PubMed]
27. Bonomo, M.; Marrani, A.G.; Novelli, V.; Awais, M.; Dowling, D.P.; Vos, J.G.; Dini, D. Surface properties of nanostructured NiO undergoing electrochemical oxidation in 3-methoxy-propionitrile. *Appl. Surf. Sci.* **2017**, *403*, 441–447. [CrossRef]
28. Nakaoka, K.; Ueyama, J.; Ogura, K. Semiconductor and electrochromic properties of electrochemically deposited nickel oxide films. *J. Electroanal. Chem.* **2004**, *571*, 93–99. [CrossRef]
29. Surca, A.; Orel, B.; Pihlar, B.; Bukovec, P. Optical, spectroelectrochemical and structural properties of sol-gel derived Ni-oxide electrochromic film. *J. Electroanal. Chem.* **1996**, *408*, 83–100. [CrossRef]

30. Moulki, H.; Faure, C.; Mihelčič, M.; Šurca Vuk, A.; Švegl, F.; Orel, B.; Campet, G.; Alfredsson, M.; Chadwick, A.V.; Gianolio, D.; et al. Electrochromic performances of nonstoichiometric NiO thin films. *Thin Solid Films* **2014**, *553*, 63–66. [CrossRef]
31. Xia, X.H.; Tu, J.P.; Zhang, J.; Wang, X.L.; Zhang, W.K.; Huang, H. Electrochromic properties of porous NiO thin films prepared by a chemical bath deposition. *Sol. Energy Mater. Sol. Cells* **2008**, *92*, 628–633. [CrossRef]
32. Balaev, D.A.; Dubrovskiy, A.A.; Krasikov, A.A.; Popkov, S.I.; Balaev, A.D.; Shaikhutdinov, K.A.; Kirillov, V.L.; Mart'yanov, O.N. Magnetic properties of NiO nano particles: Contributions of the antiferromagnetic and ferromagnetic subsystems in different magnetic field ranges up to 250 kOe. *Phys. Solid State* **2017**, *59*, 1547–1552. [CrossRef]
33. Zhang, X.K.; Yuan, J.J.; Xie, Y.M.; Yu, Y.; Yu, H.J.; Zhu, X.R.; Kuang, F.G.; Shen, H. Magnetic nature of surface and exchange bias effect in NiO nanosheets. *Appl. Phys. Lett.* **2016**, *109*. [CrossRef]
34. Cai, G.; Wang, X.; Cui, M.; Darmawan, P.; Wang, J.; Eh, A.L.S.; Lee, P.S. Electrochromo-supercapacitor based on direct growth of NiO nanoparticles. *Nano Energy* **2015**, *12*, 258–267. [CrossRef]
35. Liu, Q.; Wei, L.; Yuan, S.; Ren, X.; Zhao, Y.; Wang, Z.; Zhang, M.; Shi, L.; Li, D.; Li, A. Influence of interface properties on charge density, band edge shifts and kinetics of the photoelectrochemical process in p-type NiO photocathodes. *RSC Adv.* **2015**, *5*, 71778–71784. [CrossRef]
36. Bonomo, M.; Naponiello, G.; Venditti, I.; Zardetto, V.; Carlo, A.D.; Dini, D. Electrochemical and Photoelectrochemical Properties of Screen-Printed Nickel Oxide Thin Films Obtained from Precursor Pastes with Different Compositions. *J. Electrochem. Soc.* **2017**, *164*, H137–H147. [CrossRef]
37. Piccinin, S.; Rocca, D.; Pastore, M. Role of Solvent in the Energy Level Alignment of Dye-Sensitized NiO Interfaces. *J. Phys. Chem. C* **2017**, *121*, 22286–22294. [CrossRef]
38. Pham, T.T.T.; Saha, S.K.; Provost, D.; Farré, Y.; Raissi, M.; Pellegrin, Y.; Blart, E.; Vedraine, S.; Ratier, B.; Aldakov, D.; et al. Toward Efficient Solid-State p-Type Dye-Sensitized Solar Cells: The Dye Matters. *J. Phys. Chem. C* **2017**, *121*, 129–139. [CrossRef]
39. Ameline, D.; Diring, S.; Farre, Y.; Pellegrin, Y.; Naponiello, G.; Blart, E.; Charrier, B.; Dini, D.; Jacquemin, D.; Odobel, F. Isoindigo derivatives for application in p-type dye sensitized solar cells. *RSC Adv.* **2015**, *5*, 85530–85539. [CrossRef]
40. Nattestad, A.; Mozer, A.J.; Fischer, M.K.R.; Cheng, Y.-B.; Mishra, A.; Bäuerle, P.; Bach, U. Highly efficient photocathodes for dye-sensitized tandem solar cells. *Nat. Mater.* **2009**, *9*, 31–35. [CrossRef] [PubMed]
41. Odobel, F.; Pellegrin, Y. Recent advances in the sensitization of wide-band-gap nanostructured p-type semiconductors. Photovoltaic and photocatalytic applications. *J. Phys. Chem. Lett.* **2013**, *4*, 2551–2564. [CrossRef]
42. Wood, C.J.; Cheng, M.; Clark, C.A.; Horvath, R.; Clark, I.P.; Hamilton, M.L.; Towrie, M.; George, M.W.; Sun, L.; Yang, X.; et al. Red-absorbing cationic acceptor dyes for photocathodes in tandem solar cells. *J. Phys. Chem. C* **2014**. [CrossRef]
43. Nikolaou, V.; Charisiadis, A.; Charalambidis, G. Recent advances and insights in dye-sensitized NiO photocathodes for photovoltaic devices. *J. Mater. Chem. A Mater. Energy Sustain.* **2017**, *121*, 21077–21113. [CrossRef]
44. Bonomo, M.; Saccone, D.; Magistris, C.; Di Carlo, A.; Barolo, C.; Dini, D. Effect of alkyl chain length on the sensitizing action of substituted non symmetric squaraines for p-type dye-sensitized solar cells. *ChemElectroChem* **2017**, *4*, 2385–2397. [CrossRef]
45. Farré, Y.; Raissi, M.; Fihey, A.; Pellegrin, Y.; Blart, E.; Jacquemin, D.; Odobel, F. A Blue Diketopyrrolopyrrole Sensitizer with High Efficiency in Nickel-Oxide-based Dye-Sensitized Solar Cells. *ChemSusChem* **2017**, *10*, 2618–2625. [CrossRef] [PubMed]
46. Naik, P.; Planchat, A.; Pellegrin, Y.; Odobel, F.; Vasudeva Adhikari, A. Exploring the application of new carbazole based dyes as effective p-type photosensitizers in dye-sensitized solar cells. *Sol. Energy* **2017**, *157*, 1064–1073. [CrossRef]
47. Farré, Y.; Raissi, M.; Fihey, A.; Pellegrin, Y.; Blart, E.; Jacquemin, D.; Odobel, F. Synthesis and properties of new benzothiadiazole-based push-pull dyes for p-type dye sensitized solar cells. *Dyes Pigments* **2017**, *148*, 154–166. [CrossRef]
48. Sinopoli, A.; Wood, C.J.; Gibson, E.A.; Elliott, P.I.P. New cyclometalated iridium(III) dye chromophore complexes for p-type dye-sensitised solar cells. *Dyes Pigments* **2017**, *140*, 269–277. [CrossRef]

49. Bonomo, M.; Sabuzi, F.; Di Carlo, A.; Conte, V.; Dini, D.; Galloni, P. KuQuinones as sensitizers of NiO based p-type dye-sensitized solar cells. *New J. Chem.* **2017**, *41*, 2769–2779. [CrossRef]
50. Awais, M.; Rahman, M.; Don MacElroy, J.M.; Coburn, N.; Dini, D.; Vos, J.G.; Dowling, D.P. Deposition and characterization of NiO_x coatings by magnetron sputtering for application in dye-sensitized solar cells. *Surf. Coat. Technol.* **2010**, *204*, 2729–2736. [CrossRef]
51. Nattestad, A.; Perera, I.; Spiccia, L. Developments in and prospects for photocathodic and tandem dye-sensitized solar cells. *J. Photochem. Photobiol. C Photochem. Rev.* **2016**, *28*, 44–71. [CrossRef]
52. Flynn, C.J.; Oh, E.E.; McCullough, S.M.; Call, R.W.; Donley, C.L.; Lopez, R.; Cahoon, J.F. Hierarchically-structured NiO nanoplatelets as mesoscale p-type photocathodes for dye-sensitized solar cells. *J. Phys. Chem. C* **2014**, *118*, 14177–14184. [CrossRef]
53. Dini, D.; Halpin, Y.; Vos, J.G.; Gibson, E.A. The influence of the preparation method of NiO_x photocathodes on the efficiency of p-type dye-sensitized solar cells. *Coord. Chem. Rev.* **2015**, *304–305*, 179–201. [CrossRef]
54. Wood, C.J.; Summers, G.H.; Gibson, E.A. Increased photocurrent in a tandem dye-sensitized solar cell by modifications in push–pull dye-design. *Chem. Commun.* **2015**, *51*, 3915–3918. [CrossRef] [PubMed]
55. Wood, C.J.; Summers, G.H.; Clark, C.A.; Kaeffer, N.; Braeutigam, M.; Carbone, L.R.; D'Amario, L.; Fan, K.; Farré, Y.; Narbey, S.; et al. A comprehensive comparison of dye-sensitized NiO photocathodes for solar energy conversion. *Phys. Chem. Chem. Phys.* **2016**, *18*, 10727–10738. [CrossRef] [PubMed]
56. Farrè, Y.; Zhang, L.; Pellegrin, Y.; Planchat, A.; Blart, E.; Boujtita, M.; Hammarstrom, L.; Jacquemin, D.; Odobel, F. Second Generation of Diketopyrrolopyrrole Dyes for NiO-Based Dye-Sensitized Solar Cells. *J. Phys. Chem. C* **2016**, *120*, 7923–7940. [CrossRef]
57. Brisse, R.; Faddoul, R.; Bourgeteau, T.; Tondelier, D.; Leroy, J.; Campidelli, S.; Berthelot, T.; Geffroy, B.; Jousselme, B. Inkjet printing NiO-based p-Type dye-sensitized solar cells. *ACS Appl. Mater. Interfaces* **2017**, *9*, 2369–2377. [CrossRef] [PubMed]
58. Liu, Q.; Wei, L.; Yuan, S.; Ren, X.; Zhao, Y.; Wang, Z. The effect of Ni $(CH_3COO)_2$ post-treatment on the charge dynamics in p-type NiO dye-sensitized solar cells. *J. Mater. Sci.* **2015**, 6668–6676. [CrossRef]
59. Kong, W.; Li, S.; Chen, Z.; Wei, C.; Li, W.; Li, T.; Yan, Y.; Jia, X.; Xu, B.; Zhang, W. p-Type Dye-Sensitized Solar Cells with a CdSeS Quantum-Dot-Sensitized NiO Photocathode for Outstanding Short-Circuit Current. *Part. Part. Syst. Charact.* **2015**, *32*, 1078–1082. [CrossRef]
60. Willkomm, J.; Orchard, K.L.; Reynal, A.; Pastor, E.; Durrant, J.R.; Reisner, E. Dye-sensitised semiconductors modified with molecular catalysts for light-driven H_2 production. *Chem. Soc. Rev.* **2016**, *45*, 9–23. [CrossRef] [PubMed]
61. Kamire, R.J.; Majewski, M.B.; Hoffeditz, W.L.; Phelan, B.T.; Farha, O.K.; Hupp, J.T.; Wasielewski, M.R. Photodriven hydrogen evolution by molecular catalysts using Al_2O_3-protected perylene-3,4-dicarboximide on NiO electrodes. *Chem. Sci.* **2017**, *8*, 541–549. [CrossRef] [PubMed]
62. Meng, P.; Wang, M.; Yang, Y.; Zhang, S.; Sun, L. CdSe quantum dots/molecular cobalt catalyst co-grafted open porous NiO film as a photocathode for visible light driven H_2 evolution from neutral water. *J. Mater. Chem. A* **2015**, *3*, 18852–18859. [CrossRef]
63. Hoogeveen, D.A.; Fournier, M.; Bonke, S.A.; Fang, X.Y.; Mozer, A.J.; Mishra, A.; Bäuerle, P.; Simonov, A.N.; Spiccia, L. Photo-electrocatalytic hydrogen generation at dye-sensitised electrodes functionalised with a heterogeneous metal catalyst. *Electrochim. Acta* **2016**, *219*, 773–780. [CrossRef]
64. Antila, L.J.; Ghamgosar, P.; Maji, S.; Tian, H.; Ott, S.; Hammarström, L. Dynamics and Photochemical H_2 Evolution of Dye–NiO Photocathodes with a Biomimetic FeFe-Catalyst. *ACS Energy Lett.* **2016**, *1*, 1106–1111. [CrossRef]
65. Massin, J.; Lyu, S.; Pavone, M.; Muñoz-García, A.B.; Kauffmann, B.; Toupance, T.; Chavarot-Kerlidou, M.; Artero, V.; Olivier, C. Design and synthesis of novel organometallic dyes for NiO sensitization and photo-electrochemical applications. *Dalt. Trans.* **2016**, *45*, 12539–12547. [CrossRef] [PubMed]
66. Bonomo, M.; Dini, D. Nanostructured p-type semiconductor electrodes and photoelectrochemistry of their reduction processes. *Energies* **2016**, *9*, 373. [CrossRef]
67. Tian, H. Molecular Catalyst Immobilized Photocathodes for Water/Proton and Carbon Dioxide Reduction. *ChemSusChem* **2015**. [CrossRef] [PubMed]
68. Bonomo, M.; Dini, D.; Marrani, A.G.; Zanoni, R. X-ray photoelectron spectroscopy investigation of nanoporous NiO electrodes sensitized with Erythrosine B. *Colloids Surf. A Physicochem. Eng. Asp.* **2017**. [CrossRef]

69. Awais, M.; Dowling, D.P.; Decker, F.; Dini, D. Electrochemical characterization of nanoporous nickel oxide thin films spray-deposited onto indium-doped tin oxide for solar conversion scopes. *Adv. Condens. Matter Phys.* **2015**, *2015*, 186375. [CrossRef]
70. Awais, M.; Dowling, D.D.; Decker, F.; Dini, D. Photoelectrochemical properties of mesoporous NiO_x deposited on technical FTO via nanopowder sintering in conventional and plasma atmospheres. *Springerplus* **2015**, *4*, 564–588. [CrossRef] [PubMed]
71. Gregg, B.A. Interfacial processes in the dye-sensitized solar cell. *Coord. Chem. Rev.* **2004**, *248*. [CrossRef]
72. Sheehan, S.; Naponiello, G.; Odobel, F.; Dowling, D.P.; Di Carlo, A.; Dini, D. Comparison of the photoelectrochemical properties of RDS NiO thin films for p-type DSCs with different organic and organometallic dye-sensitizers and evidence of a direct correlation between cell efficiency and charge recombination. *J. Solid State Electrochem.* **2015**, *19*, 975–986. [CrossRef]
73. Bonomo, M.; Naponiello, G.; Carlo, A.D.; Dini, D. Characterization of Screen-Printed Nickel Oxide Electrodes for p-type Dye-Sensitized Solar Cells. *J. Mater. Sci. Nanotechnol.* **2016**, *4*, 201. [CrossRef]
74. Sakurai, K.; Fujihara, S. Fabrication of Nanostructured NiO Thick Films by Facile Printing Method and their Dye-Sensitized Solar Cell Performance. *Key Eng. Mater.* **2010**, *445*, 74–77. [CrossRef]
75. Gibson, E.A.; Awais, M.; Dini, D.; Dowling, D.P.; Pryce, M.T.; Vos, J.G.; Boschloo, G.; Hagfeldt, A. Dye sensitised solar cells with nickel oxide photocathodes prepared via scalable microwave sintering. *Phys. Chem. Chem. Phys.* **2013**, *15*, 2411–2420. [CrossRef] [PubMed]
76. Li, N.; Gibson, E.A.; Qin, P.; Boschloo, G.; Gorlov, M.; Hagfeldt, A.; Sun, L. Dou ble-layered NiO photocathodes for p-Type DSSCs with record IPCE. *Adv. Mater.* **2010**, *22*, 1759–1762. [CrossRef] [PubMed]
77. Qin, P.; Zhu, H.; Edvinsson, T.; Boschloo, G.; Hagfeldt, A.; Sun, L. Design of an Organic Chromophore for P-Type Dye-Sensitized Solar Cells. *J. Am. Chem. Soc.* **2008**, *130*, 8570–8571. [CrossRef] [PubMed]
78. Bonomo, M.; Congiu, M.; De Marco, M.L.; Dowling, D.P.; Di Carlo, A.; Graeff, C.F.O.; Dini, D. Limits on the use of cobalt sulfide as anode of p-type dye-sensitized solar cells Dedicated to Professor Roberto Federici on the occasion of his retirement. *J. Phys. D Appl. Phys.* **2017**, *50*. [CrossRef]
79. Perera, V.P.S.; Pitigala, P.; Jayaweera, P.V.V.; Bandaranayake, K.M.P.; Tennakone, K. Dye-sensitized solid-state photovoltaic cells based on dye multilayer-semiconductor nanostructures. *J. Phys. Chem. B* **2003**, *107*, 13758–13761. [CrossRef]
80. Perera, V.P.S.; Pitigala, P.K.D.D.P.; Senevirathne, M.K.I.; Tennakone, K. A solar cell sensitized with three different dyes. *Sol. Energy Mater. Sol. Cells* **2005**, *85*, 91–98. [CrossRef]
81. Awais, M.; Rahman, M.; Don MacElroy, J.M.; Dini, D.; Vos, J.G.; Dowling, D.P. Application of a novel microwave plasma treatment for the sintering of nickel oxide coatings for use in dye-sensitized solar cells. *Surf. Coat. Technol.* **2011**, *205*, S245–S249. [CrossRef]
82. Awais, M.; Dowling, D.D.; Rahman, M.; Vos, J.G.; Decker, F.; Dini, D. Spray-deposited NiO_x films on ITO substrates as photoactive electrodes for p-type dye-sensitized solar cells. *J. Appl. Electrochem.* **2013**, *43*, 191–197. [CrossRef]
83. Awais, M.; Gibson, E.; Vos, J.G.; Dowling, D.P.; Hagfeldt, A.; Dini, D. Fabrication of Efficient NiO Photocathodes Prepared via RDS with Novel Routes of Substrate Processing for p-Type Dye-Sensitized Solar Cells. *ChemElectroChem* **2014**, *1*, 384–391. [CrossRef]
84. Langmar, O.; Saccone, D.; Amat, A.; Fantacci, S.; Viscardi, G.; Barolo, C.; Costa, R.D.; Guldi, D.M. p-type Squaraines Designing to Control Charge Injection and Recombination Processes in NiO based p-type Dye-Sensitized Solar Cells. *ChemSusChem* **2017**. [CrossRef] [PubMed]
85. Bonomo, M.; Magistris, C.; Buscaino, R.; Fin, A.; Barolo, C.; Dini, D. Effect of Sodium Hydroxide Pretreatment of NiO_x Cathodes on the Performance of Squaraine-Sensitized p-Type Dye-Sensitized Solar Cells. *ChemistrySelect* **2018**, *3*, 1066–1075. [CrossRef]
86. Bonomo, M.; Barbero, N.; Matteocci, F.; Di Carlo, A.; Barolo, C.; Dini, D. Beneficial Effect of Electron-Withdrawing Groups on the Sensitizing Action of Squaraines for p-Type Dye-Sensitized Solar Cells. *J. Phys. Chem. C* **2016**, *120*, 16340–16353. [CrossRef]
87. Barbero, N.; Magistris, C.; Park, J.; Saccone, D.; Quagliotto, P.; Buscaino, R.; Medana, C.; Barolo, C.; Viscardi, G. Microwave-Assisted Synthesis of Near-Infrared Fluorescent Indole-Based Squaraines. *Org. Lett.* **2015**, *17*, 3306–3309. [CrossRef] [PubMed]

88. Galliano, S.; Novelli, V.; Barbero, N.; Smarra, A.; Viscardi, G.; Borrelli, R.; Sauvage, F.; Barolo, C. Dicyanovinyl and cyano-ester benzoindolenine squaraine dyes: The effect of the central functionalization on dye-sensitized solar cell performance. *Energies* **2016**, *9*, 486. [CrossRef]
89. Novelli, V.; Awais, M.; Dowling, D.P.; Dini, D. Electrochemical Characterization of Rapid Discharge Sintering (RDS) NiO Cathodes for Dye-Sensitized Solar Cells of p-Type. *Am. J. Anal. Chem.* **2015**, *6*, 176–187. [CrossRef]
90. Venditti, I.; Barbero, N.; Vittoria Russo, M.; Di Carlo, A.; Decker, F.; Fratoddi, I.; Barolo, C.; Dini, D. Electrodeposited ZnO with squaraine sentisizers as photoactive anode of DSCs. *Mater. Res. Express* **2014**, *1*, 15040. [CrossRef]
91. Bonomo, M.; Dini, D.; Marrani, A.G. Adsorption Behavior of I_3^- and I^- Ions at a Nanoporous NiO/Acetonitrile Interface Studied by X-ray Photoelectron Spectroscopy. *Langmuir* **2016**, *32*. [CrossRef] [PubMed]
92. Galoppini, E. Linkers for anchoring sensitizers to semiconductor nanoparticles. *Coord. Chem. Rev.* **2004**, *248*, 1283–1297. [CrossRef]
93. Chang, C.H.; Chen, Y.C.; Hsu, C.Y.; Chou, H.H.; Lin, J.T. Squaraine-arylamine sensitizers for highly efficient p-type dye-sensitized solar cells. *Org. Lett.* **2012**, *14*, 4726–4729. [CrossRef] [PubMed]
94. Jiang, J.-Q.; Sun, C.-L.; Shi, Z.-F.; Zhang, H.-L. Squaraines as light-capturing materials in photovoltaic cells. *RSC Adv.* **2014**, *4*, 32987–32996. [CrossRef]
95. Hagfeldt, A.; Boschloo, G.; Sun, L.; Kloo, L.; Pettersson, H. Dye-Sensitized Solar Cells. *Chem. Rev.* **2010**, *110*, 6595–6663. [CrossRef] [PubMed]
96. Hagfeldt, A.; Graetzel, M. Light-Induced Redox Reactions in Nanocrystalline Systems. *Chem. Rev.* **1995**, *95*, 49–68. [CrossRef]
97. Bonomo, M.; Carella, A.; Centore, R.; Di Carlo, A.; Dini, D. First Examples of Pyran Based Colorants as Sensitizing Agents of p-Type Dye-Sensitized Solar Cells. *J. Electrochem. Soc.* **2017**, *164*, F1412–F1418. [CrossRef]